

Effects of Ru substitution on electron correlations and Fermi-surface dimensionality in $\text{Ba}(\text{Fe}_{1-x}\text{Ru}_x)_2\text{As}_2$

N. Xu,¹ T. Qian,¹ P. Richard,¹ Y.-B. Shi,¹ X.-P. Wang,¹ P. Zhang,¹ Y.-B. Huang,¹ Y.-M. Xu,² H. Miao,¹ G. Xu,¹ G.-F. Xuan,³ W.-H. Jiao,³ Z.-A. Xu,³ G.-H. Cao,³ and H. Ding^{1,*}

¹Beijing National Laboratory for Condensed Matter Physics, and Institute of Physics, Chinese Academy of Sciences, Beijing 100190, China

²Materials Sciences Division, Lawrence Berkeley National Laboratory, Berkeley, California 94720, USA

³State Key Lab of Silicon Materials and Department of Physics, Zhejiang University, Hangzhou 310027, China

(Received 21 March 2012; revised manuscript received 9 July 2012; published 3 August 2012)

We report a systematic angle-resolved photoemission spectroscopy study on $\text{Ba}(\text{Fe}_{1-x}\text{Ru}_x)_2\text{As}_2$ for a wide range of Ru concentrations ($0.15 \leq x \leq 0.74$). We observed a crossover from two dimensions to three dimensions for some of the holelike Fermi surfaces with Ru substitution and a large reduction in the mass renormalization close to optimal doping. These results suggest that isovalent Ru substitution has remarkable effects on the low-energy electron excitations, which are important for the evolution of superconductivity and antiferromagnetism in this system.

DOI: [10.1103/PhysRevB.86.064505](https://doi.org/10.1103/PhysRevB.86.064505)

PACS number(s): 74.70.Xa, 71.18.+y, 74.25.Jb, 79.60.-i

I. INTRODUCTION

Superconductivity in the iron-based materials usually emerges from a magnetic state by several kinds of routes leading to very similar phase diagrams of magnetism and superconductivity. In $\text{Ba}_{1-x}\text{K}_x\text{Fe}_2\text{As}_2$ ¹ and $\text{Ba}(\text{Fe}_{1-x}\text{Co}_x)_2\text{As}_2$,² the introduction of extra hole or electron carriers shifts the chemical potential so that the sizes of the hole and electron Fermi-surface (FS) pockets evolve oppositely,³ which eventually suppresses the nesting between the hole and electron FS pockets that play a role in the formation of a spin density wave (SDW) with exotic Dirac cone dispersion⁴ in the parent compound. While it is generally believed that external pressure also changes the FS topology by modifying the chemical bonds,⁵ the role of isovalent element substitution is still debated. Various scenarios, for example changes of the FS topology by chemical pressure,⁶⁻⁸ the reduction of electron correlations,^{8,9} magnetic dilution,¹⁰ and even the addition of extra hole carriers,¹¹ have been suggested to explain the suppression of the SDW order with isovalent element substitution in the $\text{BaFe}_2(\text{As}_{1-x}\text{P}_x)_2$ and $\text{Ba}(\text{Fe}_{1-x}\text{Ru}_x)_2\text{As}_2$ systems. Surprisingly, only little attention has been devoted to answer the reversed but somehow similarly important question: How is superconductivity suppressed by increasing the substitution further than the optimal concentration?

Since single crystals can be grown for the entire phase diagram, the $\text{Ba}(\text{Fe}_{1-x}\text{Ru}_x)_2\text{As}_2$ system is ideal to investigate the suppression of the SDW order, the emergence of superconductivity, and its disappearance with isovalent substitution. We expect that the electronic structure near the Fermi level (E_F) be substantially modified by the Ru substitution. Indeed, the isovalent Ru substitution at the Fe site leads to an anisotropic lattice distortion, resulting in a strong increase of the As-Fe(Ru)-As bond angle and a decrease of the As height from the Fe(Ru) plane.^{6,12,13} The Hall coefficient, which is always negative and decreases with decreasing temperature in the parent compound BaFe_2As_2 , increases with decreasing temperature in the Ru-substituted samples and even changes sign for large Ru concentrations.¹³ With its capacity to resolve dispersive electronic states in the vicinity of E_F , angle-resolved photoemission spectroscopy (ARPES) is a

powerful tool to determine which parameters drive the system from a SDW order in BaFe_2As_2 to a nonmagnetic metallic state in BaRu_2As_2 , with superconductivity occurring at mixed composition. However, not only did previous ARPES studies not characterize the suppression of superconductivity in the overdoped regime, the conclusions drawn on the suppression of the SDW order also show a striking contrast. While Brouet *et al.* observed a decrease in the electronic correlations and significant modifications of the Fermi surface with Ru substitution,⁸ Dhaka *et al.* reported almost no changes in the FS topology and the band dispersions, which points towards a non-Fermi-surface-driven mechanism such as magnetic dilution for the origin of the SDW suppression.¹⁰

In this paper, we report ARPES results for a Ru substitution range wider than in previous studies. Our data indicate that the impact of the degradation of the nesting between hole and electron FS pockets cannot be neglected. However, the most significant changes in the electronic band structure are observed at optimal concentration and at higher Ru content. We reveal a clear crossover from two dimensions to three dimensions for some of the holelike FSs with Ru substitution accompanied by a reduction of mass renormalization, suggesting that the isovalent Ru substitution has significant effects on the low-energy electron excitations. The implications of the changes in the FS topology and the near- E_F band dispersions on the evolution of the SDW order and superconductivity are discussed.

II. EXPERIMENT

High-quality single crystals of $\text{Ba}(\text{Fe}_{1-x}\text{Ru}_x)_2\text{As}_2$ were grown by the flux method.¹⁴ The Ru concentration of the samples was determined by energy-dispersive spectroscopy x-ray and x-ray diffraction analyses with an accuracy of ~ 0.01 .¹⁴ ARPES experiments were performed at beamlines PGM and Apple-PGM of the Synchrotron Radiation Center (Wisconsin), beamline 12.0.1 of the Advanced Light Source (California), and beamline SIS of the Swiss Light Source (Switzerland) with Scienta analyzers. The energy and angular resolutions were set at 20 meV and 0.2° , respectively. The samples were cleaved *in situ* and measured at 20 K in a vacuum better than 4×10^{-11} Torr.

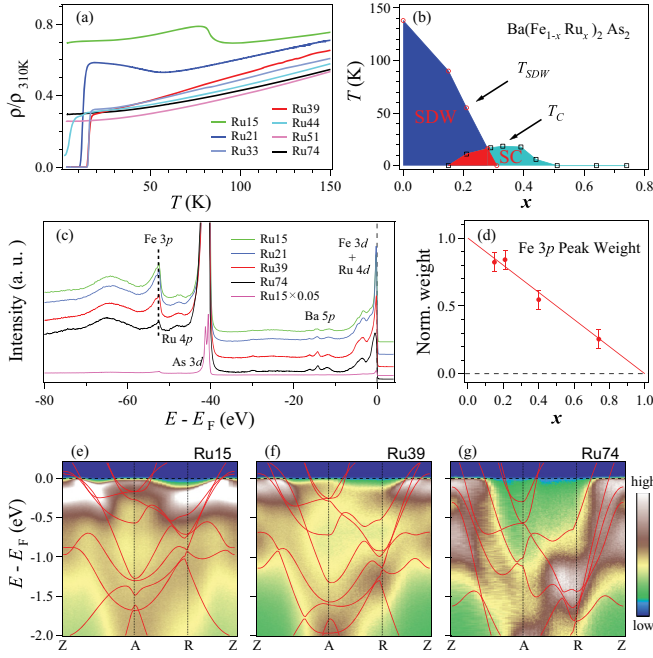


FIG. 1. (Color online) (a) Temperature dependence of the in-plane resistivity of $\text{Ba}(\text{Fe}_{1-x}\text{Ru}_x)_2\text{As}_2$ single crystals for $x = 0.15, 0.21, 0.33, 0.39, 0.44, 0.51,$ and 0.74 respectively (named Ru15, Ru21, Ru33, Ru39, Ru44, Ru51, and Ru74). (b) Phase diagram of $\text{Ba}(\text{Fe}_{1-x}\text{Ru}_x)_2\text{As}_2$ based on the resistivity data. (c) Core levels recorded with a photon energy of 195 eV. (d) Doping dependence of the Fe $3p$ ($E_b \sim 53$ eV) peak weight. (e)–(g) Intensity plot along Z-A-R-Z ($k_z = \pi$) for Ru15, Ru39, and Ru74. Nonrenormalized LDA bands are also plotted for comparison.

III. RESULTS AND DISCUSSION

The normalized resistivity data plotted in Fig. 1(a) suggest that the SDW order identified as a resistive anomaly (upturn) is gradually shifted to low temperature with Ru substitution and disappears for $x \geq 0.30$. Superconductivity emerges for $x > 0.15$, reaches its maximum transition temperature at $x \sim 0.30$, and is strongly suppressed for $x > 0.39$. The SDW temperature T_{SDW} and critical temperature T_c extracted from the resistivity data are plotted in the T - x phase diagram, Fig. 1(b). Figure 1(c) shows the shallow core levels and the valence band spectra for different Ru concentrations. The peak position of the Fe $3p$ orbital at the binding energy (E_B) of ~ 53 eV is not shifted with Ru substitution, confirming that the valence state of the Fe ions is not changed. Furthermore, the intensity of the Fe $3p$ peak extracted by integrating the peak area decreases linearly as a function of the Ru concentration and can be extrapolated to zero for BaRu_2As_2 , as shown in Fig. 1(d). In contrast, the Ru $4p$ peak at $E_B \sim 48$ eV is enhanced with increasing the Ru concentration, though it is too weak to extract accurately its intensity value.

In iron-based superconductors, most of the dispersive bands originating from the Fe $3d$ orbitals are located within 2 eV below E_F . To illustrate the effects of Ru substitution on the dispersive bands, we plot in Figs. 1(e)–1(g) the photoemission intensity along the high symmetry lines Z-A-R-Z for $x = 0.15, 0.39,$ and 0.74 , respectively. For comparison, we also plot the band structure within the local density approximation

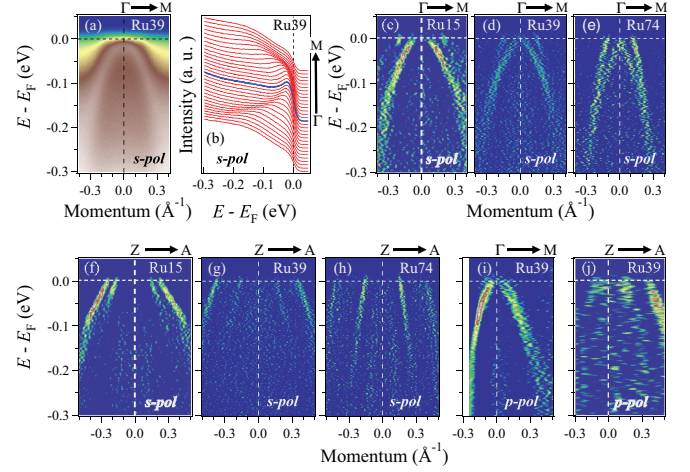


FIG. 2. (Color online) (a) ARPES intensity plot along Γ -M ($k_z = 0$) for Ru15, taken in the s -pol geometry. (b) Corresponding energy distribution curves. (c)–(e) Curvature plot of the momentum distribution curves (MDCs) along Γ -M ($k_z = 0$) in the s -pol geometry. (f)–(h) Same as (c)–(e), but along the Z-A ($k_z = \pi$) symmetry line. (i) Same as (d), but in p -pol geometry. (j) Same as (g), but in p -pol geometry.

(LDA) for $x = 0, 0.4,$ and 1 in Figs. 1(e)–1(g), respectively. While the overall bandwidth increases slightly for higher Ru concentrations as expected from band calculations, it is interesting to notice that the calculated bands do not need to be renormalized to fit the dispersive bands in the high E_B range. In contrast, the near- E_F bands are strongly renormalized, especially for $x \leq 0.39$, suggesting that the many interactions mainly affect the low-energy electron excitations.

In order to clarify the effects of Ru substitution on the low-energy excitations, we focus on the band dispersions near E_F . Figure 2(a) shows a photoemission intensity plot at the Γ point ($k_z = 0$ at the BZ center) in s -polarization geometry (s -pol) for $x = 0.39$. Figures 2(b) and 2(d) show the corresponding EDCs and the corresponding curvature plot of the momentum distribution curves (MDCs),¹⁶ respectively. One can see that the curvature plot exhibits more clearly the band dispersions near E_F . We show the curvature plots of the MDCs at the Γ and Z ($k_z = \pi$) points for $x = 0.15, 0.39,$ and 0.74 in s -pol geometry in Figs. 2(c)–2(h), respectively. As seen in Fig. 2(c), two holelike bands crossing E_F are observed at Γ for $x = 0.15$. As the Ru content increases, their Fermi momenta (k_F) become smaller and the inner band even sinks below E_F for $x = 0.39$ and 0.74 . The effect of Ru substitution is somehow opposite at the Z point. Not only do the two holelike bands cross E_F at Z for all samples, their respective k_F actually increase with the Ru concentration. These results indicate that Ru substitution changes substantially the near- E_F band structure. In addition, we observed the third predicted holelike band at the BZ center in the p -polarization geometry (p -pol). As seen in Figs. 2(i) and 2(j), the band sinks below E_F at Γ but crosses E_F at Z for $x = 0.39$.

To further clarify the evolution of the FS topology in the three-dimensional (3D) BZ with Ru substitution, we performed ARPES measurements at different k_z by varying the photon energy. Figures 3(a)–3(c) show the intensity plots integrated within ± 10 meV with respect to E_F in the k_x - k_z plane using the s -pol geometry for $x = 0.15, 0.39$ and 0.74 ,

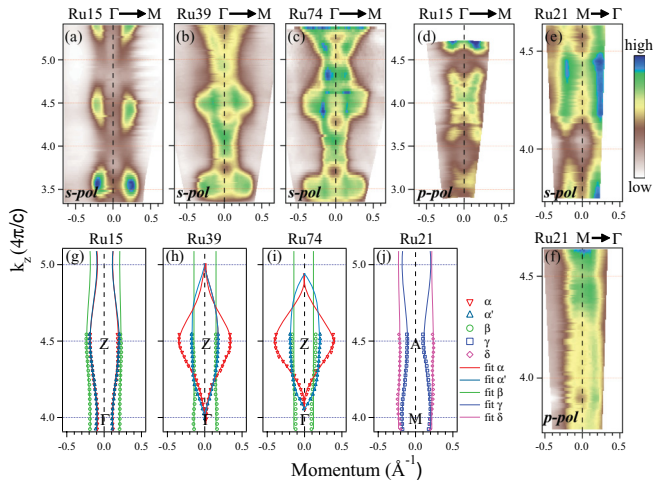


FIG. 3. (Color online) (a)–(c) Hole FS maps in k_x - k_z plane in s -pol geometry. (d) Same as (a), but in the p -pol geometry. (e) Electron FS maps in k_x - k_z plane for Ru21 in the s -pol geometry. (f) Same as (e), but obtained in the p -pol geometry. (g)–(i) Fermi momenta (symbols) of the hole bands. (j) Fermi momenta of the electron bands (symbols).

respectively. One can see two FSs clearly in the s -pol geometry. One of them (hereafter called β) keeps a quasi-2D behavior for all Ru concentrations whereas the other one (called α) exhibits clearly a crossover from 2D to 3D with Ru substitution. Figure 3(d) shows the p -pol geometry data for Ru15, in which one can see a third FS (called α'). As shown in Figs. 3(e) and 3(f), two quasi-2D electronlike FSs are distinguished at the M point in both the s -pol and p -pol geometries, with no obvious change upon Ru substitution.

The k_F of the three hole bands extracted from the MDCs are plotted in Figs. 3(g)–3(i), while the k_F for the two electron bands are given in Fig. 3(j). The results, as well as the total number of carriers estimated from the Luttinger theorem, are displayed as a function of the Ru concentration in Fig. 4(a). The hole carriers are well compensated by the electron ones at all Ru concentrations, demonstrating that the Ru substitution is isovalent, in agreement with the core-level measurements and previous ARPES studies.^{8,10} Although the carrier concentration does not change with Ru substitution, Fig. 4(a) clearly shows that the band structure evolves. In particular, there is a hole carrier transfer from the β band to the α band that occurs from low doping to higher doping, suggesting that the nesting conditions between the Γ -centered hole FS pockets and M-centered electron FS pockets are affected as well. Although other factors such as magnetic dilution should be taken into account,¹⁰ our experimental results thus suggest that the degradation of the nesting conditions may play a role in the suppression of the SDW ordering with Ru increasing.

To further illustrate the effects of the Ru substitution on the low-energy excitations, we compare the extracted dispersions of the holelike and the electronlike bands at $k_z = \pi$ for $x = 0.15$ and 0.74 in Figs. 4(b) and 4(c), respectively. The dispersions of all the bands for $x = 0.74$ are much steeper than those for $x = 0.15$. Figure 4(d) displays the extracted Fermi velocity (v_F) values at $k_z = \pi$ as a function of Ru concentration. While the v_F values in the $k_z = \pi$ plane are not obviously changed in the underdoped range, they increase

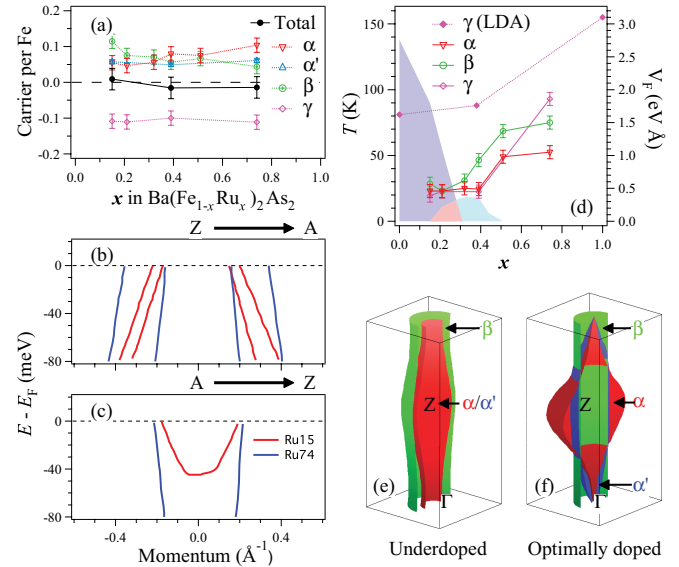


FIG. 4. (Color online) (a) Total carrier concentration (black full symbols) deduced from the contribution of individual bands (open symbols). (b)–(c) Band dispersions obtained from MDC fits of the hole and electron pockets $k_z = \pi$, respectively, for Ru15 and Ru74. (d) Doping dependence of the Fermi velocity of the α band (red line), β band (green line), and γ band (pink line) at the Z point. The full pink diamonds correspond to the Fermi velocity of the γ band predicted by our LDA calculations. The phase diagram is also plotted for convenience. (e)–(f) 3D hole FS plots for underdoped and optimally doped $\text{Ba}(\text{Fe}_{1-x}\text{Ru}_x)_2\text{As}_2$.

rapidly in the overdoped range. This effect is captured by our LDA band structure calculations,¹⁵ for which the v_F values corresponding to the γ band in the $k_z = \pi$ plane are shown in Fig. 4(d). Interestingly, the large increase in the v_F values in the overdoped regime is accompanied by an important decrease in the mass renormalization. We note that these sudden changes in v_F and in the band renormalization occur near optimal doping. From the phase diagram given in Fig. 4(d), one can see that the optimal doping for superconductivity is also close to the phase boundary of the SDW state. It is interesting to point out that similar trends in mass enhancement toward the boundary of the magnetic order phase have also been revealed in another isovalent substituted system, $\text{BaFe}_2(\text{As}_{1-x}\text{P}_x)_2$,¹⁷ and in the heavy-fermion system CeRhIn_5 by de Haas-van Alphen experiments.¹⁸ This gives us a hint that the many-body interactions, which give rise to the enhancement of the effective mass of the quasiparticles in the low doping regime, could be associated with the magnetic quantum critical point (QCP) and could play an important role in the unconventional superconductivity of these systems.¹⁹

Whether a localized or an itinerant picture is most appropriate to describe superconductivity in the Fe-based superconductors is still a matter of controversy.²⁰ Let's first assume that an itinerant picture prevails. In Figs. 4(e)–4(f), we plot the 3D hole FSs for underdoped and optimally doped $\text{Ba}(\text{Fe}_{1-x}\text{Ru}_x)_2\text{As}_2$. Our results show that the holelike β FS remains quasi-2D and is still quasinested with the electronlike FSs far beyond the superconducting dome. In contrast, the α and α' FSs become very 3D with Ru substitution. The tops of

the α and α' bands are degenerated at Γ [see Figs. 2(c) and 2(i)], suggesting that they mainly originate from the $d_{xz/yz}$ orbitals, in agreement with a recent ARPES study on the (Ba,K)Fe₂As₂ system.²¹ The enhancement of the 3D character is attributed to a stronger d - p hybridization of the transition metal atoms with As²² due to a larger spatial extension of the Ru $4d$ orbitals and a decrease of the As height.^{6,12,13} On the other hand, the quasi-2D β FS is attributed to the d_{xy} orbital, whose spatial extension is limited to the a - b plane. Our results indicate clearly that if quasineesting between the hole and electron FS pockets is the determinant factor for superconductivity in these materials, then the $d_{xz/yz}$ orbitals are mainly responsible. Within a local picture, the main interpretation for the suppression of superconductivity at high Ru content can be explained in terms of both the reduction of the electronic correlations reported in this paper and the important modifications of the local antiferromagnetic exchange constants due to the enhanced spacial extension of the Ru $4d$ orbitals and their increased hybridization with the As $3p$ orbitals due to the decrease of the As height.

IV. SUMMARY

In summary, our study of Ba(Fe_{1-x}Ru_x)₂As₂ over a wide range of doping indicates that the degradation of the nesting

conditions between the hole and electron FS pockets cannot be neglected in understanding the suppression of the SDW in this system. However, the main changes in the electronic band structure occur for Ru concentrations exceeding optimal substitution. In that regime, some hole bands become much more 3D, an effect accompanied by an increase of the Fermi velocities and a strong suppression of the electronic correlations. Our study suggests that one or many of these strong effects may play a role in the suppression of superconductivity in the high-substitution regime of Ba(Fe_{1-x}Ru_x)₂As₂.

ACKNOWLEDGMENTS

We acknowledge X. Dai, Z. Fang, Z. Pan, W. Yin, and P. C. Canfield for useful discussions. This work was supported by grants from the Chinese Academy of Sciences (Grant No. 2010Y1JB6), the Chinese Ministry of Science and Technology (Grants No. 2010CB923000 and No. 2011CBA001000), and the National Natural Science Foundation of China (Grants No. 11004232 and No. 11050110422). This work is based in part upon research conducted at the Synchrotron Radiation Center, which is primarily funded by the University of Wisconsin-Madison with supplemental support from facility users and the University of Wisconsin-Milwaukee.

*dingh@iphy.ac.cn

- ¹M. Rotter, M. Tegel, and D. Johrendt, *Phys. Rev. Lett.* **101**, 107006 (2008).
- ²A. S. Sefat, R. Jin, M. A. McGuire, B. C. Sales, D. J. Singh, and D. Mandrus, *Phys. Rev. Lett.* **101**, 117004 (2008).
- ³M. Neupane, P. Richard, Y.-M. Xu, K. Nakayama, T. Sato, T. Takahashi, A. V. Federov, G. Xu, X. Dai, Z. Fang, Z. Wang, G.-F. Chen, N.-L. Wang, H.-H. Wen, and H. Ding, *Phys. Rev. B* **83**, 094522 (2011).
- ⁴P. Richard, K. Nakayama, T. Sato, M. Neupane, Y.-M. Xu, J. H. Bowen, G. F. Chen, J.-L. Luo, N.-L. Wang, X. Dai, Z. Fang, H. Ding, and T. Takahashi, *Phys. Rev. Lett.* **104**, 137001 (2010).
- ⁵S. A. J. Kimber, A. Kreyssig, Y.-Z. Zhang, H. O. Jeschke, R. Valent, F. Yokaichiya, E. Colombier, J.-Q. Yan, T. C. Hansen, T. Chatterji, R. J. McQueeney, P. C. Canfield, A. I. Goldman, and D. N. Argyriou, *Nature Mater.* **8**, 471 (2009).
- ⁶A. Thaler, N. Ni, A. Kracher, J.-Q. Yan, S. L. Bud'ko, and P. C. Canfield, *Phys. Rev. B* **82**, 014534 (2010).
- ⁷Z. Ren, Q. Tao, S. Jiang, C.-M. Feng, C. Wang, J. H. Dai, G.-H. Cao, and Z.-A. Xu, *Phys. Rev. Lett.* **102**, 137002 (2009).
- ⁸V. Brouet, F. Rullier-Albenque, M. Marsi, B. Mansart, M. Aichhorn, S. Biermann, J. Faure, L. Perfetti, A. Taleb-Ibrahimi, P. Le Fèvre, F. Bertran, A. Forget, and D. Colson, *Phys. Rev. Lett.* **105**, 087001 (2010).
- ⁹E. Abrahams and Q. M. Si, *J. Phys.: Condens. Matter* **23**, 223201 (2011).
- ¹⁰R. S. Dhaka, C. Liu, R. M. Fernandes, R. Jiang, C. P. Strehlow, T. Kondo, A. Thaler, J. Schmalian, S. L. Bud'ko, P. C. Canfield and A. Kaminski, *Phys. Rev. Lett.* **107**, 267002 (2011).

- ¹¹Z.-R. Ye, Y. Zhang, M. Xu, Q.-Q. Ge, F. Chen, J. Jiang, B.-P. Xie, J.-P. Hu, and D.-L. Feng, [arXiv:1105.5242](https://arxiv.org/abs/1105.5242).
- ¹²S. Sharma, A. Bharathi, S. Chandra, V. R. Reddy, S. Paulraj, A. T. Satya, V. S. Sastry, Ajay Gupta, and C. S. Sundar, *Phys. Rev. B* **81**, 174512 (2010).
- ¹³F. Rullier-Albenque, D. Colson, A. Forget, P. Thuery, and S. Poissonnet, *Phys. Rev. B* **81**, 224503 (2010).
- ¹⁴W.-H. Jiao, Q. Tao, J.-K. Bao, Y.-L. Sun, C.-M. Feng, Z.-A. Xu, I. Nowik, I. Felner, and G.-H. Cao, *Europhys. Lett.* **95**, 67007 (2011).
- ¹⁵I. R. Shein and A. L. Ivanovskii, *Phys. Solid State* **52**, 8 (2010).
- ¹⁶P. Zhang, P. Richard, T. Qian, Y.-M. Xu, X. Dai, and H. Ding, *Rev. Sci. Instrum.* **82**, 043712 (2011).
- ¹⁷H. Shishido, A. F. Bangura, A. I. Coldea, S. Tonegawa, K. Hashimoto, S. Kasahara, P. M. C. Rourke, H. Ikeda, T. Terashima, R. Settai, Y. Onuki, D. Vignolles, C. Proust, B. Vignolle, A. McCollam, Y. Matsuda, T. Shibauchi, and A. Carrington, *Phys. Rev. Lett.* **104**, 057008 (2010).
- ¹⁸H. Shishido, R. Settai, H. Harima, and Y. Onuki, *J. Phys. Soc. Jpn.* **74**, 1103 (2005).
- ¹⁹P. Gegenwart, Q.-M. Si, and F. Steglich., *Nature Phys.* **4**, 186 (2008).
- ²⁰P. Richard, T. Sato, K. Nakayama, T. Takahashi, and H. Ding, *Rep. Prog. Phys.* **74**, 124512 (2011).
- ²¹X.-P. Wang, P. Richard, Y.-B. Huang, H. Miao, L. Cevey, N. Xu, Y.-J. Sun, T. Qian, Y.-M. Xu, M. Shi, J.-P. Hu, X. Dai, and H. Ding, *Phys. Rev. B* **85**, 214518 (2012).
- ²²L.-J. Zhang and D. J. Singh, *Phys. Rev. B* **79**, 174530 (2009).